Detection and Identification of Sub-Millimeter Films of Organic Compounds on Environmental Surfaces Using Short-Wave Infrared Hyperspectral Imaging: Algorithm Development Using a Synthetic Set of Targets

Shai Kendler, Izhar Ron, Shay Cohen, Raviv Raich, *Senior Member, IEEE*, Ziv Mano, and Barak Fishbain

***Abstract*— An algorithm for identifying organic materials using a short-wave infrared hyperspectral imager is presented. The main achievement of this algorithm is to automatically locate a clear reference within the scene, without any prior knowledge regarding the scene, and use it to extract the spectral signature of the target material. This step is required for sub-millimeter organic films since they absorb only a small fraction of the light. Therefore, the obtained spectral signature is a product of the target material and the clean background spectral signature. Detection rate as high as 90% was achieved for three model compounds in a controlled scene with false alarm rate lower than 1% in our model scene, containing a set of synthetic targets (ST). These findings lay the groundwork for further study of real (and probably more complex compared to the ST) cases and materials, required for the development of a detection system that will be capable of locating trace amounts of polluting chemicals to enable improved prevention, regulation, and mitigation acts.**

***Index Terms*— Algorithm, clean-reference, detection, hyperspectral, SWIR.**

I. Introduction

SINCE the industrial revolution in the late 18th and 19th centuries, environmental pollution has become a significant threat to the wellbeing of humans and other living creatures on earth. Environmental pollution is a result of the release of a large variety of chemicals to the environment [1]–[3]. These chemicals are released in different routes and can migrate between different microenvironments [2], [4], [5] (surface, soils, water, and air), which further increases their effect on the environment.

The best way to handle this issue is by emission reduction, mainly by regulation and modern industrial and agriculture technologies [6]. However, it seems that complete reduction of emission may be a difficult task and pollutants removal and containment have to be considered as well [1], [7], [8]. Naturally, such remediation actions are efficient if they are employed in polluted locations. These locations are known in some cases, but sometimes remediation efficacy is degraded due to the lack of information regarding the location of the pollution [9]. Such situations call for the application of remote sensing techniques, as they offer practical and efficient tools for detection of pollution. Previously we demonstrated the use of external-cavity quantum cascade laser for the detection of organic vapor and gases [10]. Detection and identification of gaseous plumes in an urban area using infrared hyperspectral imager was also reported previously [11]. Errico *et al.* developed a method based on the combination of Synthetic-Aperture Radar (SAR) and optical imaging for the detection of illegal agriculture waste disposal [12]. In 1999 Ferrier [13], and later in 2008 Choe *et al.* [14] used an airborne hyperspectral imager (HSI) in the visible and short-wave IR (VIS-SWIR) to detect pollution (inorganic minerals) caused by mining. These examples of detection of environmental pollutants using HSI-SWIR are examples for classical use of HSI-SWIR for imaging the surface of the earth that was pioneered by Goetz back in the early 80's [15]. Over the years, a considerable effort has been directed towards hardware development [16], correction for atmospheric distortions [17], and data interpretation [18]. Applications related to non-destructive, stand-off investigation from a close distance, such as art conservation [19], food industry [20]–[22], biological materials [23], and biomedicine [24] are constantly developing. Target material identification can be performed using several different algorithms [18]. These algorithms can detect

Manuscript received November 18, 2018; accepted December 7, 2018. Date of publication December 11, 2018; date of current version March 7, 2019. This work was supported by the Israeli Government as a part of the general funding of IIBR. The associate editor coordinating the review of this paper and approving it for publication was Prof. Guiyun Tian. *(Corresponding author: Shai Kendler.)*

S. Kendler is with the Environmental Physics Department, Israel Institute for Biological Research, Ness Ziona 74100, Israel, and also with the Department of Environmental, Water and Agricultural Engineering, Faculty of Civil & Environmental Engineering, Technion–Israel Institute of Technology, Haifa 32000, Israel (e-mail: shaik@iibr.gov.il).

I. Ron is with the Physical Chemistry Department, Israel Institute for Biological Research, Ness Ziona 74100, Israel (e-mail: izharr@iibr.gov.il).

S. Cohen is with the Environmental Physics Department, Israel Institute for Biological Research, Ness Ziona 74100, Israel (e-mail: shayc@iibr.gov.il).

R. Raich is with the School of Electrical Engineering and Computer Science, Oregon State University, Corvallis, OR 97331-5501 USA (e-mail: raich@eecs.oregonstate.edu).

Z. Mano and B. Fishbain are with the Department of Environmental, Water and Agricultural Engineering, Faculty of Civil and Environmental Engineering, Technion–Israel Institute of Technology, Haifa 32000, Israel (e-mail: ziv.mano@campus.technion.ac.il; fishbain@technion.ac.il).

Digital Object Identifier 10.1109/JSEN.2018.2886269

a target material based on its unique spectral signature, which is measured separately under controlled conditions. Detection is possible even in cases where the target material is covering part of the pixel (sub-pixel), and the measured spectrum is a linear combination (linear mixing) of the background and the target material [18]. Non-linear mixing situations have got less attention, and algorithms addressing such cases often rely on prior knowledge or assumptions regarding the scene [25]. In this paper, we describe an algorithm that identifies minute amounts of organic materials (sub-millimeter films) on typical surfaces that may occur in populated environments. Detection of thin films and grains in complex scenes is a very challenging task. This is mainly attributed to the fact that these targets absorb only a small fraction of the incoming light. We will refer to such targets as "weak absorbers" (WA). A description of the light and matter interaction for WA will be presented and it will be shown that similarly to gaseous plumes [11], the obtained spectrum is a product of the material of interest and the underlying background – non-linear mixing. The primary challenge is the occurrence of many kinds of surfaces in the scene, and hence many different backgrounds may be measured. Identifying a clean background surface without any prior knowledge, to extract the spectrum of a target material that covers it, is a challenging task. An automatic and efficient method for background removal, with no prior knowledge, followed by target identification, was developed in this work, using a ground-based HSI that enabled the collection of data from different targets at distances shorter than 30 meters.

II. The Interaction Between Light and Target Materials

An illustration of the interaction between light and 95 WA targets is shown in Fig. 1 and described by

$$I_{i,j}(\lambda) = I_0(\lambda) \times \left(a_{i,j} \times B_{i,j}(\lambda) \times T_{i,j}^2(\lambda) + \left(1 - a_{i,j}\right) \times B_{i,j}(\lambda)\right) \quad (1)$$

where $I_{i,j}(\lambda)$ is the reflected radiation from a specific pixel in position (PIX_{ij}) i,j in the scene, $I_0(\lambda)$ is the incident radiation, $a_{i,j}$ is the fractional coverage (between 0 and 1) of PIX_{ij} by the target material film, $B_{i,j}(\lambda)$is the spectral signature of the clean background also present in PIX_{ij}, $T_{i,j}^2(\lambda)$ is the square of the spectral transmittance through the layer of target material that is present in PIX_{ij} (the square accounts for the two times light passes through this absorbing layer). This model above can be corrected for atmospheric interference, as required for remote sensing applications that are beyond the scope of the current work. If $B_{i,j}(\lambda)$ is known, the reflectance spectrum can be obtained through

$$R_{i,j}(\lambda) = \frac{I_{i,j}(\lambda)}{I_0(\lambda) \times B_{i,j}(\lambda)} = a_{i,j} \times T_{i,j}^2(\lambda) + \left(1 - a_{i,j}\right) \quad (2)$$

where $R_{i,j}$ is the background-corrected reflectance of the material in PIX_{ij}.

Examples of the spectral features obtained with three WA organic films using (2) are given in Fig. 1.

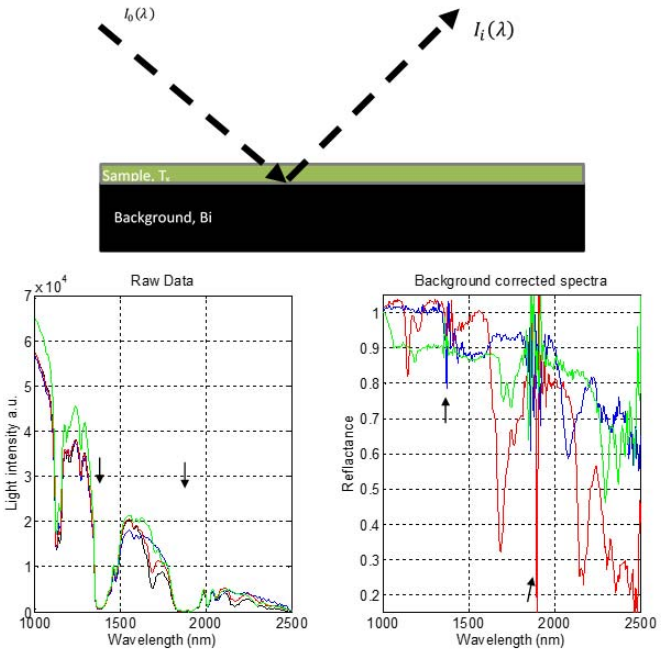

Fig. 1. Top: An illustration of the interaction between light and a thin (sub-millimeter) layer of material. See text for more details. Bottom: raw data measured from clean ceramic tile (black) polystyrene (red), sugar (blue) and silicone oil films deposited on the ceramic tile (left) and background corrected spectra of polystyrene (red), sugar (blue) and silicone oil films deposited on the ceramic tile (right). Due to strong absorption by the atmoshere at ~1400 and 1800nm (marked with small arrows on the bottom left figure) the obtained spectra at these regions is extremely noisy.

The number of possible background materials is large, and in most cases, there is no prior knowledge regarding the type of surfaces that may be found in the scene. In cases where the analysis can be performed manually by a trained operator, a simple approach may be used in which one assumes, using prior knowledge, that a specific pixel in the scene is a clean background which is similar to the area underlying the target of interest. For example, if one suspects that a surface made out of cement is polluted, a clean piece of cement can be used as a background. Then, following our procedure, the spectral signature of the material covering the surface in every pixel $R_{i,j}(\lambda)$ will be extracted and compared to a reference spectrum of the target material (T). The need for an input from an expert is problematic as it may be slow, pricy, and biased by the operator personnel judgment. Hence, an automatic algorithm for background removal was developed.

III. Experiments

A. Test Targets

Target spots were prepared by placing 0.5, 1, and 1.5 gr of target materials on a 10*10 cm square of cardboard, ceramic tile, and ply wood. Sugar was deposited on the surfaces from concentrated sugar solution. Following the evaporation of water, a thin film of sugar is formed on the surface. Polystyrene was deposited from methyl ethyl ketone solution. Silicon oil (polydimethylsiloxane, PDMS) was placed directly on the surfaces. The resulting film thicknesses were approximately 50, 100 and 150 micrometer. The total number of target spots was thirty three as shown in fig 2. Silicone targets 9, 12, 15 are

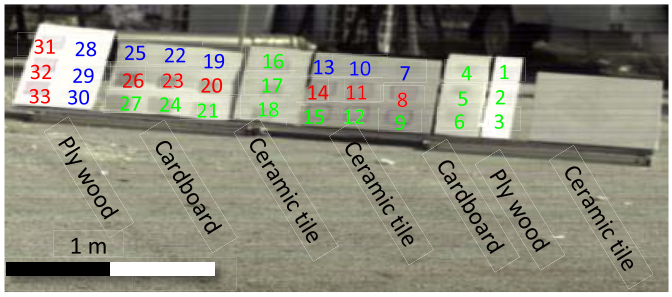

Fig. 2. Test targets used for in this experiment. Targets containing silicone oil are marked in green color, sugar in blue and polystyrene in red. Targets 1, 4, 13, 14, 15, 25, 26, 27, 28 and 31 contain 0.5 gr of the target materials, targets 2, 5, 10, 11, 12, 22, 23, 24, 29 and 32 contain 1 gr of the target materials. The rest of the samples contained 1.5gr of the target materials.

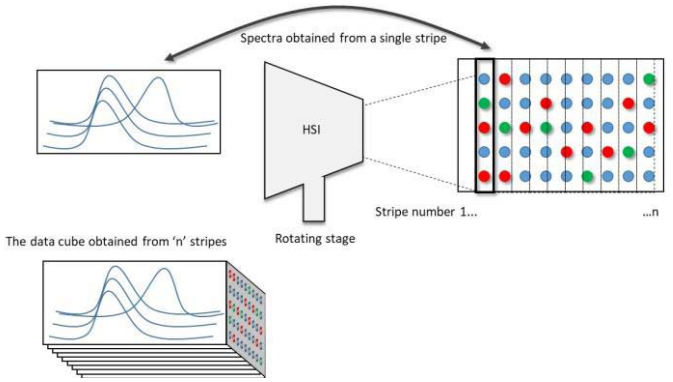

Fig. 3. An illustration of the HSI measurement process see text for more detail.

larger then 10*10 cm since these samples were difficult to confine spatially. This can be visually observed on the ceramic tile and in the analysis as a stain on the bottom part of the tile. The HSI distance to targets was about 30 meters.

It is worthwhile to note that these three targets do not have extraordinary environmental impact. We chose to work with these materials as they are readily available stable chemicals that can be used to develop the identification algorithm. Unfortunately, the number and variety of polluting chemicals is enormous [3]. Application of the proposed approach will require adaptation of this method for the required set of target materials. Similarly, our targets were placed on flat evenly illuminated surfaces. This convenient configuration was designed to evaluate the maximum potential of this approach, and it is possible that realistic surfaces will be more challenging and will pose a greater challenge that will be addressed in a future study.

B. Reference Spectra Measurements

The reference spectra of the target materials were measured before the HSI measurements using a filed portable non-imaging spectrometer (FieldSpec4^{TM} from ASD). The measurements were performed in the VIS-SWIR range (350-2500nm), sampling interval/resolution in the VIS are 1.4nm/3nm and in the SWIR 1.1nm/10nm. We used the sun as the light source. The measurements were performed using a fiber optic probe. Blank measurements were performed on a sea-sand and aluminum surface before placing the target materials measurements on these surfaces.

HSI Description: The HSI used for this work was SWIR-CL-400-N25E from Specim (Finland). This is a line-scanner type HSI measuring in the spectral range 1000-2500nm, spectral sampling interval/resolution are 5.6nm/12nm. The HSI is equipped with a 56mm, an F2 lens having a 9.6° field of view. The HSI is mounted on a rotating stage. Typical exposure time was 10ms and frame rate was 30 fps, using the sun as the light source. Before each measurement, the HSI automatically measured the dark current signal, and the recorded data is corrected using this measurement. Radiometric calibration was also applied automatically using the supplied control software and calibration parameters from Specim. The HSI is equipped with an MCT focal plane array sensor having 384 by 288 pixels. Light enters the sensor through a 30 μm slit and dispersed by the spectrometer to 288 wavelengths ("channels") creating a single stripe of the scene. The data cube is constructed by scanning 'n' stripes by rotating the system 'n' times during the measurement to create m*n*l data cube. The number of stripes is chosen by the operator according to the scene size, in this experiment n = 500 in most cases (see fig 3). The other two dimensions of the data cube are fixed by the size of the HSI sensor (m = 384, l = 288). Area of interest can be cropped from the entire cube for the analysis.

C. Computational Detail

1) Automatic Background Removal Techniques:

a) Global automatic background removal (GABR): In this method, the HSI data, i.e., a data cube containing n*m pixels * l spectral channels, is analyzed in n*m cycles. In each cycle, the algorithm picks one of the pixels as a possible clean background and using (2) removes the background's contribution from the entire cube. At the second stage, the background-reduced cube (BRcube) is analyzed to locate the presence of the target material, using an algorithm that will be described in the next section. This analysis is repeated m*n times until all pixels are used as possible clean background. This means that a single cube generates m*n BRcubes that are analyzed. It is therefore understood that computation time using GABR approach is long.

b) Segmented automatic background removal (SABR): In SABR, the cube is divided into smaller cubes (sub-cubes) which are analyzed separately using the GABR method. At the final stage, the analysis results are combined. The underlying assumption behind SABR is that seeking a clean background pixel in the vicinity of the target pixel increases the chance to find a relevant clean background and reduces the chance for false alarm. A byproduct of the SABR is a significant reduction in computation time in comparison to the GABR method.

c) Focused background removal (FBR): In this method, a possible clean background area (n'*m' pixels * l spectral channels) within the entire cube is predefined to the algorithm as input. From that point, FBR acts similarly to GABR and uses every pixel in the predefined area as a possible background for the entire cube. This approach reduces computation time significantly compared to GABR and is less prone to false

positive alarms. FBR can be used effectively in combination with SABR. At the first stage, the entire scene is analyzed, and suspected areas are located using SABR. At the second stage areas containing positive hits are isolated from the scene together with adjacent clean pixels. This segment of the scene is then re-analyzed using FBR where the middle of the scene is taken as the possible background area.

d) Target material identification: Each BRcube generated in the first step, using any of the above methods, is inspected to locate the presence of target materials. Inspection is performed by computing the correlation between the spectrum recorded in each pixel in the BRcube to the known spectral signature of the target material which was measured in advance, i.e., a reference spectrum. The correlation is calculated separately in two regions of the spectrum. These regions can be optimized for each application. In this work, the spectral ranges that were selected are SWIR1 $=$ 1495 $-$ 1787nm and SWIR2 $=$ 1994 $-$ 2386nm. A positive hit is recorded if the calculated correlation in SWIR1 and in SWIR 2 crosses pre-determined threshold values (ThSWIR1 and ThSWIR2). These threshold values are chosen by measuring true positive and false alarm rates at different threshold values when a cube of a scene containing a known set of targets is analyzed. Positive hit (true or false) is recorded in cases where a target material is identified even in a single pixel. Identification results (positives and negative) are recorded in every step, and this procedure is repeated according to the selected background removal method. The identification algorithm is illustrated in fig 4. Computation time is highly affected by the scene size, computing power and quality of the computer code. Using a personal computer running a Matlb code, analyzing a scene containing ~40000 pixel with the GABR method requires about an hour. The FBR and SABR methods are about 500 times faster. Hence, these two methods may be implemented for near real-time analysis.

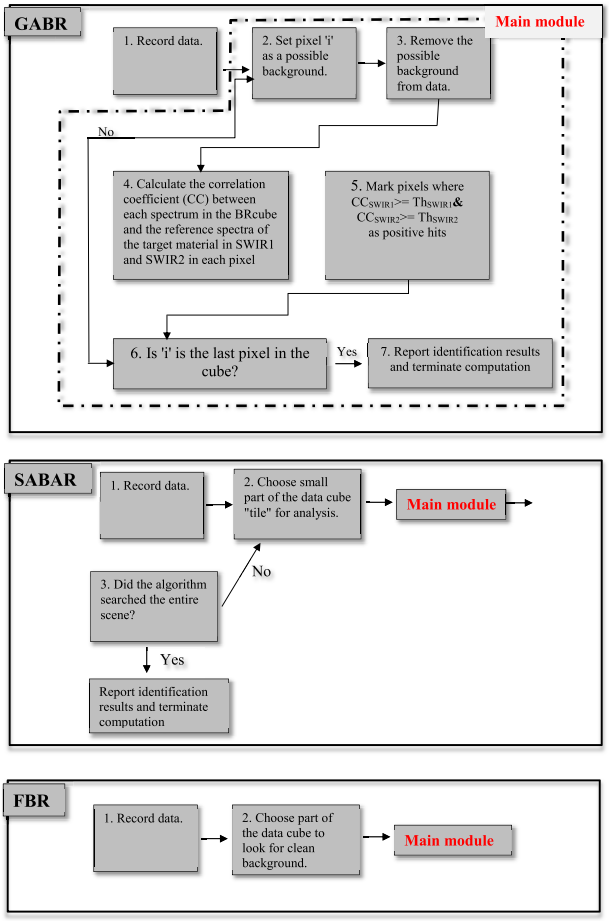

Fig. 4. An illustration of the analysis process using GABAR (up), SABAR (middle) and FBR methods.

IV. Results and Discussion

A. Algorithm Performance Using the FBR Method

Fig 5 depicts the analysis results when using almost the entire scene (top), targets area (middle) and only a portion of a single target (bottom) as possible clean backgrounds in FBR method. Positive hits for sugar is presented using blue color, silicone oil in green and polystyrene in red on top of a grayscale image of the entire scene. Using a large portion of the scene as a possible background is identical to GABR method and results in a high false alarm rate. Using the target area as possible background significantly reduces the false alarm rate, while focusing on an isolated target gives the best results. It is worthwhile to note that the positive hits for silicone on ceramic tile (marked as 'CT' in fig 5) are all true-positive. We note that the target material is a viscous liquid and wasn't successfully confined to perfect rectangular hence a large stain was formed. The nature of the false alarms was investigated, and the spectra that gave rise to these false positive hits (marked by red and blue circles in Fig 5) are presented in Fig 6 (dashed blue and red lines) compared to true-positive spectra (solid blue and red lines). For polystyrene, it seems that polymeric material in the scene has a similar spectrum to that of polystyrene. False alarms for sugar were obtained from clean cardboard, accounting for partial similarity between the obtained spectra and that of sugar. In both cases, there are some differences between the spectra, and it is reasonable to expect that by increasing the threshold values, false alarms will decrease. However, it is important to verify that by tightening the identification criteria, the true-positiverate is acceptable. For that purpose, the true and false positive rates were calculated at different threshold values (fig 7). Note that true-positive percentage is calculated as the percentage of the identified targets. Successful target identification is defined once at least one pixel in the target is declared as a positive hit. This approach is suitable for the detection of contaminating material and not for mapping its distribution. This approach increases the chance for detection, but at the same time, it increases the chances of false alarm. Using the methods described in this work for mapping requires further research that also accounts for the target size and shape.

As expected, increasing the threshold values decreased the false alarm rate, but also reduced the true-positive rate. The amount of this effect on each material was slightly different, for example when setting $\mathrm{Th_{SWIR1}} = \mathrm{Th_{SWIR2}} = 0.92$, %TP for polystyrene is 100 without any false-positive hits. At the same threshold values %TP for silicone oil is only 80% without any false-positive hits,for sugar %TP is 88%

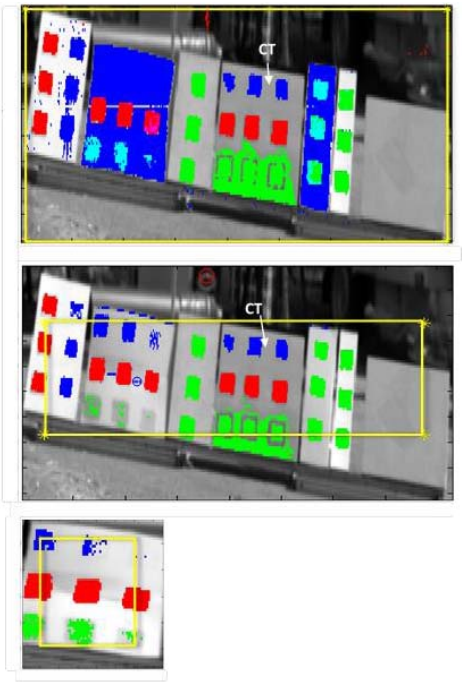

Fig. 5. Analysis results using the FBR method. Possible background area in each calculation is marked using a yellow rectangle: the entire scene (top), most of the targets (middle) and a portion of a single target (bottom). Positive hits for sugar are presented using blue color, silicone oil in green and polystyrene in red. Th_{SWIR1} and Th_{SWIR1} are 0.82 and 0.87, respectively. The red and blue circles in the middle frame mark some of the locations where false positive hits were recorded for sugar and polystyrene. The spectra measured from these locations are presented in the next figure.

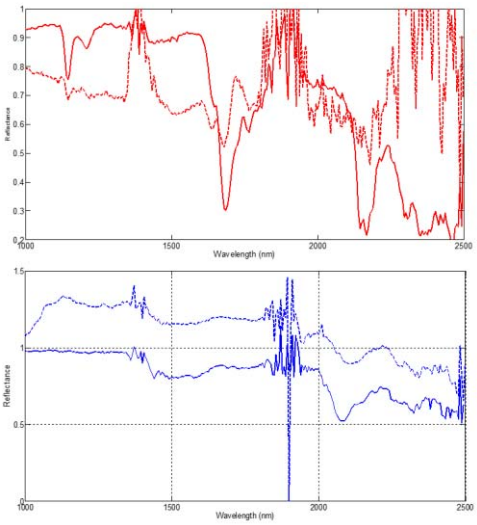

Fig. 6. Spectra of polystyrene (top) and sugar (bottom) extracted from the scene shown in fig 5. Spectra that relate to true positive hits are in solid line while spectra that was recorded as false positive are presented in dashed line.

with 30 misidentified pixels. Decreasing the thresholds to ThSWIR1 = ThSWIR2 = 0.8 resulted in 100% detection at the cost of a few thousand false positive hits. The high false positive rate of sugar is a result of its spectrum, which exhibits only one strong peak, assigned to a hydroxyl (-OH) group [26]. While this peak's exact location and shape is material dependent, it is a ubiquitous chemical group found in many materials, including wood. Relying on this single broad peak for identification is challenging.

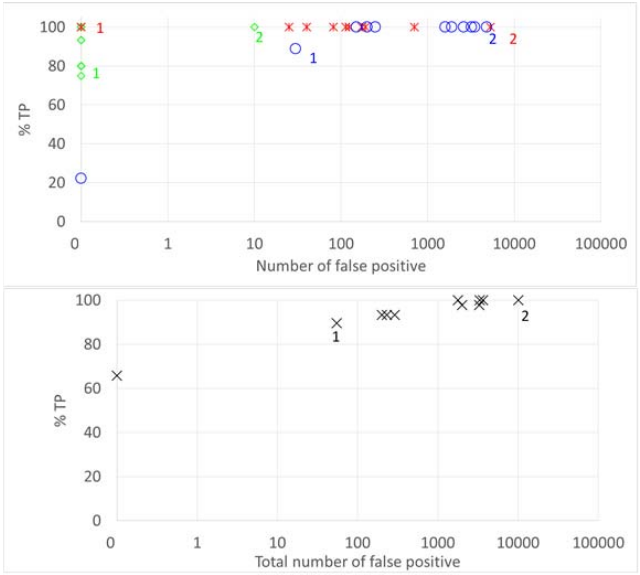

Fig. 7. Top: Percent of accurately identified targets (%TP) vs. number of false positive pixels for sugar (blue), silicone oil (green) and polystyrene (red), calculated at several threshold values. Bottom: percent of total identified targets vs. total number of false positive hits, calculated at several threshold values. 'X' axis are in log scale. Two cases are discussed in detail in the text, 1: $Th_{SWIR1} = Th_{SWIR2} = 0.92$ and 2: $Th_{SWIR1} = Th_{SWIR2} = 0.92$. Percentage TP obtained in these two cases is marked in the figure.

Since at this stage of the research we are not dealing with the actual materials, but rather with model substances, it makes sense to optimize the algorithm for the total %TP and false alarms, as shown in the bottom part of fig 7. It is shown that a total TP rate of 90%, at the cost of 56 misidentified pixels (~0.05%) is achieved. Such performance may are anacceptable result for many applications, but for highly demanding applications involving expensive mitigation processes or extremely toxic materials, improved performance may be required. Another good reason to continue to optimize the algorithm is that it is expected that real life targets will be harder to detect due to uneven and not optimal illumination, as well as interference by naturally occurring materials in the environment. Therefore, we repeated the same measurement using the FBR method on small portions in the scene, which included a single target each time. In this technique, 100% detection rate is possible without any false positive hits – an example for this result is given in the bottom part of fig 5. The main issue with this approach is the need for intensive intervention by the operator. This is avoided by applying the SABR technique, which is described in the next section.

B. Algorithm Performance Using SABR Method

A similar analysis was performed using the SABR method for background removal. A graph showing the TP rate as a function of the total number of false positive hits is shown in fig 8. It is clear from the graph that SABR outperforms FBR. For example, at TP rate = 90%, no misidentified pixels were recorded using $Th_{SWIR1} = 0.87$ and $Th_{SWIR2} = 0.89$. If misidentification of 37 pixels is tolerable (out of more than 40 kilopixels), TP rate is 96% at $Th_{SWIR1} = 0.87$ and $Th_{SWIR2} = 0.82$.

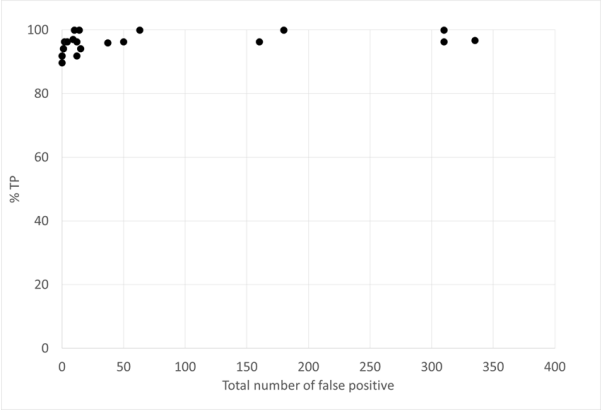

Fig. 8. Top: Percent of accurately identified targets (%TP) vs. number of false positive hits when using the SABR method for background removal.

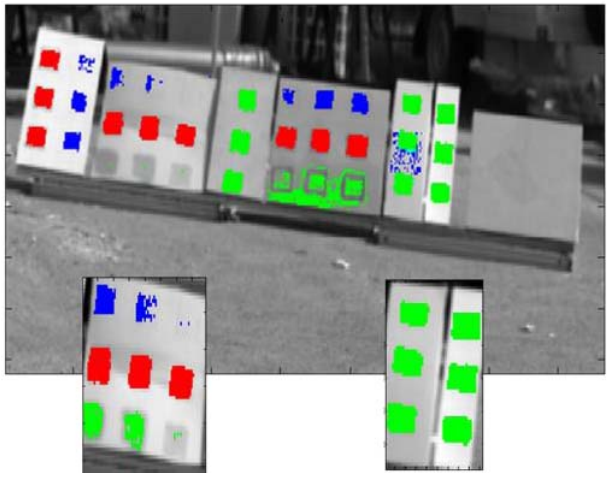

Fig. 9. Analysis results using the combination of SABR (top) and GABR (bottom) on specific areas in the scene. See text for more details.

Additional benefits of the SABR method is a significant reduction in computation time. On our computer and codes, SABR is about 500 times faster than GABR and FBR. SABR slices the scene based on proximity and thus may introduce some errors since some diversity may occur within a small area. This may be overcome by analyzing the scene with SABR using high thresholds for identification and then focusing on suspected areas using FBR, taking the center region of the suspected area as possible clean background (see for example bottom frame in fig 5). Alternatively, in cases of small areas, one can use the GBAR method. Fig 9 depicts this process: SABR was applied using relatively high thresholds ($Th_{SWIR1} = 0.87$, $Th_{SWIR2} = 0.89$), in the following step GABR method was applied to verify the results in small parts of the scene where positive hits were recorded. Since the inquired areas in the second stage are uniform, lower thresholds ($Th_{SWIR1} = 0.82$, $Th_{SWIR2} = 0.87$) can be used to increase the TP rate without the risk for a high false positive rate. An algorithm that utilizes the SABR method, followed by GABR or FBR methods may be a good starting point for the future development of near real time algorithm for line scanners HSI. This type of sensors scans the scene slice by slice, which is the kind of input that is needed for this algorithm.

V. Conclusions

The ongoing issue of environmental pollution requires new methods to detect polluting materials. This challenge is essential to improve prevention, regulation and mitigation acts. This paper describes the development of an algorithm that efficiently analyzes raw data, obtained by SWIR/HSI, in a scene that was designed to model real-life short-range operation. The algorithms enable to detect submillimeter organic materials. We focused on innocent substances as a first step in testing out approach's ability to discriminate between different organic compounds and the underlying surface of the surrounding environment. This scenario is highly challenging since the light absorption by these targets is very low, and the obtained results contain a significant contribution of the background materials. Several methods were presented for the removal of this contribution to facilitate accurate identification of our model compounds. The algorithm, presented in this paper, is capable of automatically, and without any prior knowledge regarding the scene to locate clean background. This feature is valuable when performing measurements in diverse conditions in the field which is often the case of environmental monitoring. The obtained results are very promising and serve as an excellent starting point for studying real materials and scenarios using mobile systems. Future study will include implementation of alternative methods to increase the probability for detection while maintaining low false alarm rate. As mentioned earlier the primary challenge, in this case, is the weak absorption of the target material and the fact that most of the scene is clean. In such case implementing techniques such as multivariate curve resolution (MCR), that rely on principal component analysis (PCA or its variant) should be done carefully. Another challenge will be automating the determination of the cut-off levels of the two thresholds. Such optimization might provide the capability to make an informed trade-off between detection rate and false alarm rate, as required for different applications.

References

[1] B. Huang, C. Lei, C. Wei, and G. Zeng, "Chlorinated volatile organic compounds (Cl-VOCs) in environment—Sources, potential human health impacts, and current remediation technologies," *Environ. Int.*, vol. 71, pp. 118–138, Oct. 2014. [Online]. Available: https://www.sciencedirect.com/science/article/pii/S0160412014001974

[2] C. D. Evans, D. Monteith, and D. M. Cooper, "Long-term increases in surface water dissolved organic carbon: Observations, possible causes and environmental impacts," *Environ. Pollut.*, vol. 137, no. 1, pp. 55–71, Sep. 2005. [Online]. Available: https://www.sciencedirect.com/science/article/pii/S0269749105000540

[3] K. C. Jones and P. de Voogt, "Persistent organic pollutants (POPs): State of the science," *Environ. Pollut.*, vol. 100, nos. 1–3, pp. 209–221, Aug. 1999. [Online]. Available: https://www.sciencedirect.com/science/article/pii/S0269749199000986

[4] B. Halling-Sørensen *et al.*, "Occurrence, fate and effects of pharmaceutical substances in the environment—A review," *Chemosphere*, vol. 36, no. 2, pp. 357–394, Jan. 1998, doi: 10.1016/S0045-6535(97)00354-8.

[5] F. Wania, J.-E. Haugen, Y. D. Lei, and D. Mackay, "Temperature dependence of atmospheric concentrations of semivolatile organic compounds," *Environ. Sci Technol.*, vol. 32, no. 8, pp. 1013–1021, Mar. 1998, doi: 10.1021/es970856c.

[6] M. A. Berry and D. A. Rondinelli, "Proactive corporate environmental management: A new industrial revolution," *Acad. Manage. Executive*, vol. 12, no. 2, pp. 38–50, May 1998. [Online]. Available: https://www.jstor.org/stable/4165456

[7] E. J. Bouwer and A. J. Zehnder, "Bioremediation of organic compounds–putting microbial metabolism to work," *Trends Biotechnol.*, vol. 11, no. 8, pp. 360–367, Aug. 1993, doi: 10.1016/0167-7799(93)90159-7.

[8] K. T. Semple, B. J. Reid, and T. R. Fermor, "Impact of composting strategies on the treatment of soils contaminated with organic pollutants," *Environ. Pollut.*, vol. 112, no. 2, pp. 269–283, Apr. 2001, doi: 10.1016/S0269-7491(00)00099-3.

[9] M. Triassi, R. Alfano, M. Illario, A. Nardone, O. Caporale, and P. Montuori, "Environmental pollution from illegal waste disposal and health effects: A review on the 'triangle of death,'" *Int. J. Environ. Res. Public Health.*, vol. 12, no. 2, pp. 1216–1236, Jan. 2015, doi: 10.3390/ijerph120201216.

[10] R. Aharoni, I. Ron, N. Gilad, A. Manor, Y. Arav, and S. Kendler, "Real-time stand-off spatial detection and identification of gases and vapor using external-cavity quantum cascade laser open-path spectrometer," *Opt. Eng.*, vol. 54, no. 6, pp. 067103-1–067103-9, Jun. 2015, doi: 10.1117/1.OE.54.6.067103.

[11] E. Hirsch and E. Agassi, "Detection of gaseous plumes in IR hyperspectral images using hierarchical clustering," *Appl. Opt.*, vol. 46, no. 25, pp. 6368–6374, Sep. 2007. [Online]. Available: http://www.telops.com.cn/First/paper_01.pdf

[12] A. Errico *et al.*, "Detection of environmental hazards through the feature-based fusion of optical and SAR data: A case study in Southern Italy," *Int. J. Remote Sens.*, vol. 36, no. 13, pp. 3345–3367, doi: 10.1080/01431161.2015.1054960.

[13] G. Ferrier, "Application of imaging spectrometer data in identifying environmental pollution caused by mining at Rodaquilar, Spain," *Remote Sens. Environ.*, vol. 68, no. 2, pp. 125–137, May 1999, doi: 10.1016/S0034-4257(98)00105-9.

[14] E. Choe, F. van der Meer, F. van Ruitenbeek, H. van der Werff, B. de Smeth, and K.-W. Kim, "Mapping of heavy metal pollution in stream sediments using combined geochemistry, field spectroscopy, and hyperspectral remote sensing: A case study of the Rodalquilar mining area, SE Spain," *Remote Sens. Environ.*, vol. 112, no. 7, pp. 3222–3233, Jul. 2008, doi: 10.1016/j.rse.2008.03.017.

[15] A. F. H. Goetz, G. Vane, J. E. Solomon, and B. N. Rock, "Imaging spectrometry for Earth remote sensing," *Science*, vol. 228, no. 4704, pp. 1147–1153, Jun. 1985, doi: 10.1126/science.228.4704.1147.

[16] T. Cocks, R. Jenssen, A. Stewart, I. Wilson, and T. Shields, "The HyMap airborne hyperspectral sensor: The system, calibration and performance," in *Proc. 1st EARSeL Workshop Imag. Spectrosc.*, Zürich, Switzerland, M. Schaepman, D. Schläpfer, and K. I. Itten, Eds. Paris, France: EARSeL, Oct. 1998 pp. 37–43. [Online]. Available: http://artefacts.ceda.ac.uk/neodc_docs/Hymap_specs.pdf

[17] A. Brook and E. Ben Dor, "Supervised vicarious calibration (SVC) of hyperspectral remote-sensing data," *Remote Sens. Environ.*, vol. 115, no. 6, pp. 1543–1555, Jun. 2011, doi: 10.1016/j.rse.2011.02.013.

[18] D. Manolakis and G. S. Shaw, "Detection algorithms for hyperspectral imaging applications," *IEEE Signal Process. Mag.*, vol. 19, no. 1, pp. 29–43, Jan. 2002, doi: 10.1109/79.974724.

[19] F. G. France, "Advanced spectral imaging for noninvasive microanalysis of cultural heritage materials: Review of application to documents in the U.S. Library of Congress," *Appl. Spectrosc.*, vol. 65, no. 6, pp. 565–574, Jun. 2011, doi: 10.1366/11-06295.

[20] A. A. Gowen, C. P. O'Donnell, P. J. Cullen, G. Downey, and J. M. Frias, "Hyperspectral imaging—An emerging process analytical tool for food quality and safety control," *Trends Food Sci. Technol.*, vol. 18, no. 12, pp. 590–598, Dec. 2007, doi: 10.1016/j.tifs.2007.06.001.

[21] S. Kawano, S. Saranwong, and F. Terada, "Rapid, easy-handling system for NIR compositional analysis of non-homogenized milk using a test tube," in *Proc. 11th Int. Conf. Near Infr. Spectrosc.*, Córdoba, Spain, A. Garrido-Varo and A. M. C. Davies, Eds. Chichester, U.K.: NIR Publications, 2004, pp. 77–80.

[22] R. Calvini, A. Ulrici, and J. M. Amigo, "Practical comparison of sparse methods for classification of Arabica and Robusta coffee species using near infrared hyperspectral imaging," *Chemometrics Intell. Lab. Syst.* , vol. 146, no. 15, pp. 503–511, Aug. 2015, doi: 10.1016/j.chemolab.2015.07.010.

[23] M. Manley, "Near-infrared spectroscopy and hyperspectral imaging: Non-destructive analysis of biological materials," *Chem. Soc. Rev.*, vol. 43, no. 24, pp. 8200–8214, Dec. 2014, doi: 10.1039/c4cs00062e.

[24] R. A. Schultz, T. Nielsen, J. R. Zavaleta, R. Ruch, R. Wyatt, and H. R. Garner, "Hyperspectral imaging: A novel approach for microscopic analysis," *Cytometry*, vol. 43, pp. 239–247, Mar. 2001, doi: 10.1002/1097-0320(20010401)43:4%3C239::AID-CYTO1056%3E3.0.CO;2-Z.

[25] J. M. Bioucas-Dias *et al.*, "Hyperspectral unmixing overview: Geometrical, statistical, and sparse regression-based approaches," *IEEE J. Sel. Topics Appl. Earth Observ. Remote Sens.*, vol. 5, no. 2, pp. 354–379, Apr. 2012. [Online]. Available: http://ieeexplore.ieee.org/stamp/stamp.jsp?tp=&arnumber=6200362&isnumber=6204107

[26] K. Mitsui, T. Inagaki, and S. Tsuchikawa, "Monitoring of hydroxyl groups in wood during heat treatment using NIR spectroscopy," *Biomacromolecules*, vol. 9, no. 1, pp. 286–288, Feb. 2008, doi: 10.1021/bm7008069.

Shai Kendler received the Ph.D. degree in physical chemistry from the Hebrew University of Jerusalem. He studied optical and mass spectrometry of van der Waals clusters in supersonic jet. After completing his Ph.D. studies in 1996, he moved to the Israel Institute for Biological Research, Ness Ziona, Israel, and focused on field portable detection using thermal analysis, optical and ion mobility spectrometry. In 2005, he was a Visiting Scholar with the University of Michigan, Ann Arbor, MI, USA, where he studied MEMS for SVOC vapor separation and detection. He is currently a Visiting Scholar with the Environmental, Water and Agricultural Engineering Division, Faculty of Civil and Environmental Engineering, Technion–Israel Institute of Technology. He is interested in developing new methods for HSI data interpretation and applying them for precise agriculture.

Izhar Ron received the Ph.D. degree in chemistry from the Weizmann Institute of Science. He studied electron transport though biomolecules in a solid state configuration. After completing his Ph.D. studies in 2010, he joined the Israel Institute for Biological Research, Ness Ziona, Israel, and focused on point detection in the field using various technologies including vibrational spectroscopy and ion mobility spectrometry.

Shay Cohen is currently a qualified computer technician. He joined the Israel Institute for Biological Research, Ness Ziona, Israel, in 2001, and since 2001 he has been involved in complex environmental measurements.

Raviv Raich (S'98–M'04–SM'17) received the B.Sc. and M.Sc. degrees from Tel Aviv University, Tel Aviv, Israel, in 1994 and 1998, respectively, and the Ph.D. degree from the Georgia Institute of Technology, Atlanta, GA, USA, in 2004, all in electrical engineering. From 1999 to 2000, he was a Researcher with the Communications Team, Industrial Research, Ltd., Wellington, New Zealand. From 2004 to 2007, he was a Post-Doctoral Fellow with the University of Michigan, Ann Arbor, MI, USA. He has been with the School of Electrical Engineering and Computer Science, Oregon State University, Corvallis, OR, USA, as an Assistant Professor, from 2007 to 2013, and has been an Associate Professor since 2013. His research interests include statistical signal processing and machine learning. He currently serves as the Chair of the Machine Learning for Signal Processing Technical Committee of the IEEE Signal Processing Society. He was an Associate Editor for the IEEE TRANSACTIONS ON SIGNAL PROCESSING from 2011 to 2014.

Ziv Mano is currently pursuing the bachelor's degree with the Environmental, Water and Agricultural Engineering Division, Faculty of Civil and Environmental Engineering, Technion–Israel Institute of Technology. She is interested in hyperspectral imaging data interpretation using model base machine learning techniques.

Barak Fishbain received the Ph.D. degree in EE (real-time multi-dimensional signal processing) from Tel-Aviv University. Following his post-doctoral studies at the University of California at Berkeley and role as an Associate Director of the Integrated Media Systems Center, University of Southern California, Los Angeles, CA, USA, Prof. Fishbain has been appointed as an Assistant Professor with the Faculty of Civil and Environmental Engineering, Technion–Israel Institute of Technology. His research focuses on enviromatics, a new research field that aims at devising machine learning methods and mathematical models for better understanding built and natural complex environments. The goal is to harness new machine learning, mathematical models with engineering principles, computing, and networked sensing data analytics for enhancing the efficiency, resiliency, and sustainability of infrastructure and natural systems.